Thickness dependence of photo-induced light scattering in photorefractive ferroelectrics

2008 J. Phys.: Condens. Matter 20 075225

(http://iopscience.iop.org/0953-8984/20/7/075225)

J. Phys.: Condens. Matter **20** (2008) 075225 (8pp) doi:10.1088/0953-8984/20/7/075225

Thickness dependence of photo-induced light scattering in photorefractive ferroelectrics

Mikhail Goulkov[1], Kathrin Bastwöste[2], Stefan Möller[2], Mirco Imlau[2] and Manfred Wöhlecke[2]

[1] Institute of Physics, Science Avenue 46, 03650, Kiev-39, Ukraine
[2] Department of Physics, University Osnabrück, Barbarastraße 7, D-49069 Osnabrück, Germany

Received 31 July 2007, in final form 13 December 2007
Published 31 January 2008
Online at stacks.iop.org/JPhysCM/20/075225

Abstract
Stationary and dynamic properties of photo-induced light scattering (PILS) have been studied as a function of the photorefractive crystal thickness. A mono-exponential growth of the scattering amplification coefficient as well as a deceleration of the scattering recording dynamics is found with increasing crystal thickness. The experimental data set is analyzed by considering scattering centers located (i) in the crystal *bulk* or (ii) *near to the crystal surface*. By comparing experimental and theoretical results we can conclude that the major contribution to the output scattering signal originates from a thin crystal region frontier to the surface of light incidence (near-surface). The deceleration of the scattering dynamics is interpreted as the result of the competition between differently recorded noisy photorefractive gratings.

(Some figures in this article are in colour only in the electronic version)

1. Introduction

Photo-induced light scattering [1] (PILS) is a nonlinear phenomenon accompanying the propagation of laser beams in nonlinear optical materials [2–6]. The scattering is seeded by coherent optical noise, which is amplified at the expense of the pump beam via nonlinear wave mixing processes, like two-wave (2WM) or four-wave mixing (4WM), respectively. In particular, PILS has been discovered in photorefractive crystals [7–10]. Here, wave mixing occurs on noisy refractive index gratings. Such gratings are self-recorded via the interference between the pump beam and noisy waves in the presence of the photorefractive effect. The wave mixing theory yields a simple analytical solution for the output scattering intensity I_s

$$I_s = I_{so} e^{(\Gamma - \alpha) l}, \tag{1}$$

where I_{so} is the initial scattering intensity of the noisy waves, Γ is the gain factor of the nonlinear optical medium, l is the length of the wave interaction, and α the absorption coefficient. The relation given in equation (1) is derived in the undepleted-pump-beam approximation; i.e., it is suggested that the intensity of the directly transmitted pump beam is only slightly affected by the appearing scattered light.

The study of the PILS phenomenon is accompanied by different aspects for applications and fundamental studies, respectively. For instance, it allows us to elaborate methods to either suppress or to enhance the scattering [11–13]. At the same time, it enables a deep macro- and microscopic insight into major properties of nonlinear optical materials [14–17]. Moreover, it can be applied to determine the conditions for an optical amplification in the frame of 2WM and 4WM, respectively [8, 10].

In the last decades, great effort was made to apply the wave mixing theory to the PILS phenomena. These studies provided the determination of Γ as a function of material properties and particular scattering geometries. Also, the temporal and angular behavior of the scattering were numerically modeled [18–23]. According to equation (1), the properties of the seed scattering are represented by the angular distributions of the parameters I_{so} and l, respectively. The latter is defined by the propagation length of the scattered waves within the crystal bulk of thickness L. A dominating contribution of the surface (or near-surface) scattering, i.e., $l = L$, was often assumed [1, 18, 23].

A distinct statement on the interaction length l, however, requires a systematic theoretical and experimental study. First

systematic studies on the properties of initial scattering were focused on the photorefractive ferroelectric crystal strontium barium niobate doped with cerium, $Sr_{0.61}Ba_{0.39}Nb_2O_6$:Ce (SBN:Ce). Investigations were performed as a function of external electric fields and over a wide temperature range covering the ferroelectric–paraelectric phase transition. The results allowed us to derive a model for the scattering centers in SBN. It was concluded that scattering centers are related to refractive index singularities induced at domain walls by internal electric fields [24, 25]. Remarkably, such scattering centers must be located in the crystal bulk or at least within the near-surface region of the crystal—and not on its surfaces. Hence, the model of bulk scattering centers can be a very likely case in nonlinear optical materials, as well. It is therefore required to accommodate the models for bulk and surface scattering centers in photorefractive ferroelectrics.

In this contribution the thickness dependence of the PILS phenomenon is studied in the photorefractive crystals SBN:Ce and $LiNbO_3$:Fe. Temporal and stationary properties of the wide-angle PILS resulting from 2WM amplification are investigated in SBN:Ce. Analytical solutions for two theoretical limiting cases of (i) *bulk* and (ii) *near-surface* scattering centers are derived and the effective interaction length l is determined. The generality of our simple approach is verified by additional experiments with parametric PILS via 4WM in $LiNbO_3$:Fe.

2. Model considerations

PILS is considered in photorefractive crystals as the result of the following processes. The incident laser beam is scattered on optical inhomogeneities and mechanical scratches located on the surface and/or in the volume of the crystal. Components of coherent noise with wavevectors $\mathbf{k}_{si}(\theta_s)$ originate from such scattering centers and propagate at different angles θ_s. Such noisy waves serve as a seed or initial scattering for the PILS phenomenon. The seed waves interfere with the transmitted pump beam $\mathbf{k}_p$ ($\theta_p = 0°$) yielding the elementary light patterns $\mathbf{K}_i = \mathbf{k}_{si} - \mathbf{k}_p$. The spatial light distribution is transferred into a modulation of the refractive index with amplitude Δn via the photorefractive effect [26]. Wave mixing on the recorded gratings results in an amplification of a part of the scattered light at the expense of the pump beam. It is obvious that the pump beam is much stronger than a single scattering component and gratings remain with rather low modulation depth. We recall that the wave mixing theory in the undepleted-pump approximation yields equation (1) as a simple expression for the PILS intensity in the steady state. It has been shown that equation (1) can be successfully applied for the quantitative analysis of PILS in different materials [29, 28, 27] if the gain factor $\Gamma(\theta_s)$, the initial scattering intensity $I_{so}(\theta_s)$ and the effective interaction length $l(\theta_s)$ are taken as angular dependent functions. The output scattering pattern is composed by scattered waves propagating at different angles θ_s, which are amplified via wave mixing. The properties of the angular distribution of PILS reflect whether two (2WM) or four waves (4WM) are involved in the light amplification process. Wide-angle and angle-selective (or parametric) scattering phenomena are therefore distinguished.

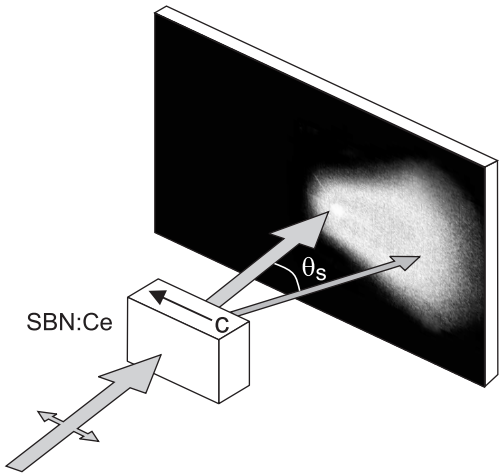

Figure 1. Experimental setup for the observation of the wide-angle PILS in the SBN:Ce crystal. Coherent illumination is performed by a single beam of extraordinary polarization ($\lambda = 514.5$ nm). The scattering is monitored at the angle $\theta_s = 15°$. The crystal's c-axis is in the plane of incidence. The thickness of SBN samples is 0.3, 0.5, 1, 1.5, 2, 3 and 3.5 mm.

Wide-angle PILS results from 2WM processes on refractive index gratings which are spatially shifted with respect to the incoming light pattern. The scattering is amplified in the direction opposite to the grating shift. As a result a rather diffusive light lobe can be observed on a viewing screen behind the crystal. A typical example of the wide-angle PILS, also designated as *beam fanning*, was investigated in SBN for the first time [1]. In this crystal, the light interference and refractive index patterns are shifted by $\pi/2$ to each other which is caused by diffusion charge transport. At the same time, the linear electro-optic coefficient r_{333} provides pronounced light scattering from an extraordinarily polarized pump beam which incidences normal to the polar c-axis (figure 1). The distribution of the wide-angle PILS in SBN is perfectly described by equation (1) where $\Gamma(\theta_s)$ describes the 2WM amplification on an elementary grating $\mathbf{K}_i$. The validity of this approach was proven in the optical spectral range $\lambda = 450$–650 nm and from room temperature up to the ferroelectric–paraelectric phase transition temperature [27, 15].

In photorefractive crystals with a local response where the stationary energy exchange on unshifted gratings via 2WM is not possible, the coherent noise can be alternatively amplified via 4WM processes. It results in the angle-selective (or parametric) PILS consisting from various conical surfaces differently oriented in space [9, 10]. One of the most efficient processes of parametric PILS appears in $LiNbO_3$:Fe crystals by illumination with a pair of extraordinarily polarized pump beams. In contrast to SBN, $LiNbO_3$:Fe possesses a local photorefractive response owing to the dominating photovoltaic charge transport [30]. The scattering yields one ring and two vertical arcs on the viewing screen as shown in figure 7(a). The light polarizations of the scattered light and of the pump

beams are identical. According to the general classification of the parametric PILS phenomenon [10], the scattering is assigned to the *ee–ee* type. It results from elementary 4WM processes between two pump and two scattered waves meeting the phase-matching conditions $\mathbf{k}_{p1} \pm \mathbf{k}_{p2} = \mathbf{k}_{s1} \pm \mathbf{k}_{s2}$, where the positive sign corresponds to the ring and the negative one to the arcs. A detailed theoretical and experimental description of this scattering can be found in [29, 10]. It was shown that the intensity distribution in the scattering pattern can also be described by equation (1), where $\Gamma(\theta_s)$ describes 4WM processes responsible for this type of scattering.

In general, different scattering waves may contribute to the output scattering signal $I_s(\theta_s)$ measured at the particular angle θ_s. These waves originate from different scattering sources in the crystal bulk. According to equation (1), the amplification of the initial scattering strongly depends on the interaction length l. Hence, the contribution of different waves to $I_s(\theta)$ depends on the location of the scattering center within the crystal. Below, two limiting approaches will be discussed: (A) the *bulk* scattering model, which accounts for the contribution from all scattering sources distributed in the entire crystal volume, and (B) the *near-surface* scattering model, considering only scattering centers located at the surface and/or in a thin crystal region frontier to the incident light.

2.1. Bulk scattering

In the case of scattering sources distributed in the crystal bulk of thickness L the following simplified model assumptions are made.

(i) The distribution of bulk scattering centers is divided into a multitude of equal thin layers $S_i(l_i)$ of thickness $\lambda \ll \delta l \ll L$. The layers are oriented normally to the incident pump beam and homogeneously arranged along the propagation coordinate $l_i = i\delta l$, where i is the layer number, as shown in figure 2(a).

(ii) The output scattering intensity, $I_s(\theta_s)$, is determined in the far field at a distance $D \gg L$ from the crystal. It is the result of all scattering components originating from different layers S_i and propagating close to the angle θ_s.

(iii) The efficiency of the initial scattering $\eta(\theta_s)$ and the gain factor $\Gamma(\theta_s)$ are equal for all scattering components contributing to $I_s(\theta_s)$ from layers of different positions l_i.

Because of losses of the pump beam caused by optical absorption and PILS processes, the initial intensity of the local seed components $I_{so,i}$ should decrease with l_i from layer to layer,

$$I_{so,i}(l_i, \theta_s) = \eta(\theta_s) I_p(l_i) = \eta(\theta_s) I_p(0) e^{-\{\Gamma(\theta_s)+\alpha\} l_i}, \qquad (2)$$

where $I_p(0)$ and $I_p(l_i)$ are pump intensities for the first layer and layer l_i, respectively.

The initial intensity of the scattering component $I_{so,i}(l_i, \theta_s)$ emerging at l_i is amplified at the expense of the pump beam and is partially depleted due to the optical absorption during its propagation along the depth $(L - l_i)$. This gives the intensity $I_{s,i}(\theta_s)$, which finally contributes to the total PILS signal in the far field with the output intensity I_s. Although the value

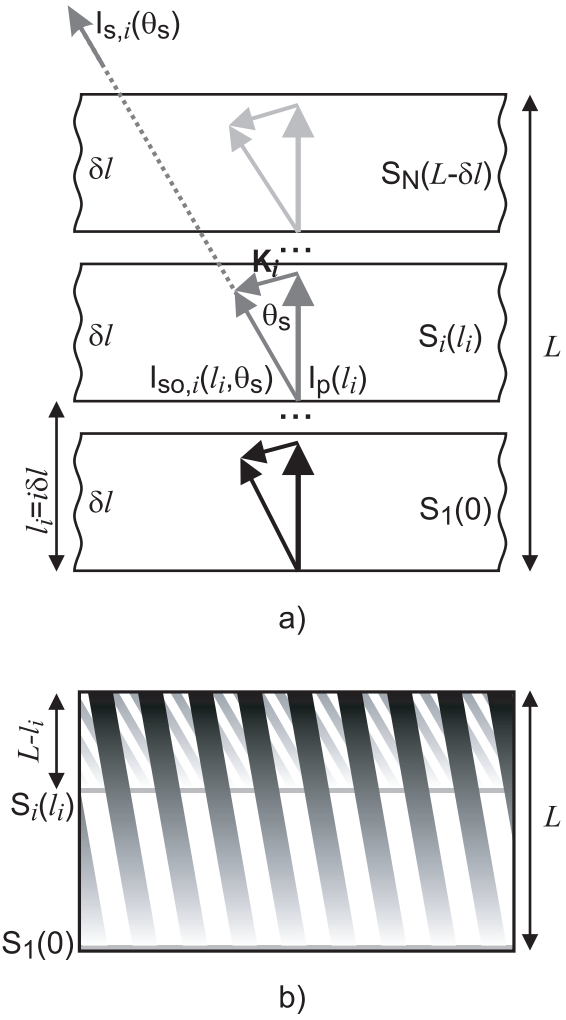

Figure 2. (a) Scattering in the vicinity of the angle θ_s emerging from different layers S_i of the crystal. The pump ($\mathbf{k}_p$) and scattering waves ($\mathbf{k}_{si}$) with the intensities I_p and $I_{so,i}$ and the photorefractive grating $\mathbf{K}_i$ are shown by the corresponding vectors for the first, the ith and the last scattering layer. $I_{s,i}(\theta_s)$ denotes the output intensity emerging from layer i at an angle θ_s. (b) Two noisy gratings are recorded by the pump beam with different components of the near-surface and bulk scattering emerging from the first and from the ith layer, respectively. Light and dark fringes elongated from the layer position to the output surface of the crystal indicate the thickness of the corresponding photorefractive gratings.

Γ for the particular angle θ_s is constant, the coupling length $(L - l_i)$ depends on the layer coordinate l_i. This results in different contributions of waves from different scattering layers $S_i(l_i)$ to the output PILS signal:

$$I_{s,i}(\theta_s) = I_{so,i}(l_i, \theta_s) e^{\{\Gamma(\theta_s)-\alpha\}\{L-l_i\}}. \qquad (3)$$

The far-field intensity of the stationary PILS $I_s(\theta_s)$ results from an integration of equation (3) with respect to l_i in the limits $\{0, L\}$ and $\Gamma = \Gamma_{stat}$ ($t \gg \tau_{di}$). Here, the constant τ_{di} is the Maxwell relaxation time. Correspondingly, the far-field intensity of $I_{so}(\theta_s)$ is determined from the integral of equation (3) with $\Gamma = 0$ ($t \to 0$). The ratio of these values is the scattering amplification coefficient, which depends on

the crystal thickness as follows:

$$m_s = \frac{I_s}{I_{so}} = \frac{\sinh(\Gamma L)}{\Gamma L}. \quad (4)$$

Equation (4) is deduced under the assumption of independent contributions of different bulk scattering components to the PILS signal, i.e., grating competition effects are neglected.

2.2. Near-surface scattering

Here, we take into account only the seed scattering originating from the surface and/or the near-surface of the crystal, i.e., from layers frontier to the incident light. Thus, contributions to PILS from scattering layers in the bulk are neglected.

The thickness $(L - l_i)$ of a photorefractive grating $\mathbf{K}_i$ recorded by the pump beam and a scattering component depends on the position of the corresponding scattering layer $S_i(l_i)$ (see figure 2(b)). The grating thickness approaches L for near-surface scattering and decreases with l_i for bulk scattering. Considering the simultaneous recording of gratings with scattered waves from different layers, a minor contribution of gratings recorded with bulk scattering centers to PILS can be expected due to the following facts:

(i) an exponential reduction of the scattering amplification with the location depth of the scattering centers;
(ii) an effective suppression of the bulk-originating PILS by the stronger near-surface-originating PILS.

The first factor appears because the light amplification is exponentially dependent on the effective coupling strength. The light scattered from near-surface layers possesses the largest value ΓL, while the product $\Gamma(L - l_i)$ corresponding to the bulk scattering decreases proportionally to the depth.

The second factor can be due to the competition between photorefractive gratings corresponding to different scattering waves and characterized by different spatial frequencies and/or different phases. In this competition, the noisy gratings of the largest thickness have an advantage, because of the higher grating contrast. As an illustration, two gratings corresponding to the scattering originating on the first and on the ith layer are sketched in figure 2(b). The grayscale gradient in the gratings fringes depicts the increase of the contrast as a function of the thickness caused by the scattering amplification. For a better presentation gratings with considerably different spatial frequencies are chosen. It is clear, that stronger scattering corresponds to the grating with higher contrast. Therefore, the near-surface scattering enhanced on thicker gratings is able to erase efficiently the thinner gratings recorded by the bulk scattering. The larger the layer coordinate l_i the higher is the suppression of the corresponding scattering components.

All this together should provide the major contribution of the near-surface scattering to the output PILS signal, which equals

$$I_s(\theta_s) = \eta(\theta_s) I_p(0) e^{\{\Gamma(\theta_s) - \alpha\} L}. \quad (5)$$

In this case the initial scattering intensity ($t = 0$) is the same as in the bulk scattering model.

$$I_{so}(\theta_s) = \eta(\theta_s) I_p(0) e^{-\alpha L}. \quad (6)$$

The ratio $m_s = I_s(\theta_s)/I_{so}(\theta_s)$ yields a simple exponential dependence of the scattering amplification coefficient on the crystal thickness

$$m_s = e^{\Gamma L}. \quad (7)$$

Here we should note that a possible contribution from non-coherent scattering is neglected in equation (4) and thus in equation (7). This is particularly reasonable for photorefractive crystals with a pronounced amplification of the scattered light. The effect of interactions between different scattered waves is also neglected, because of its negligible contribution to the total scattering signal [19, 21, 23].

In conclusion, the *bulk* and *near-surface* scattering center models predict a different dependence of the scattering amplification coefficient m_s on the crystal thickness L. We have therefore experimentally studied the stationary and dynamic properties of the PILS phenomenon in photorefractive crystals as a function of the crystal thickness.

3. Experimental results and discussion

First, the wide-angle PILS induced by a single pump beam was studied in SBN:Ce (0.04 mol%) grown by the Czochralski technique. Seven samples of thickness L from 0.3 to 3.5 mm were cut from the same boule perpendicular to the a-axis. The samples were electrically poled following the field-cooling procedure [31]. This provides the largest value of the spontaneous polarization P_s and a stable polar structure at room temperature. The unexpanded extraordinarily polarized beam from an argon–krypton ion laser ($\lambda = 514.5$ nm, $d_{FWHM} = 2.6$ mm) impinged upon a crystal normally to its input face. A low pump intensity $I_p = 2.8$ kW m^{-2} was chosen to prevent optical heating of the crystal due to absorption. Independent absorption measurements give $\alpha = (1.8 \pm 0.2)$ cm^{-1} for all SBN samples at the used pump wavelength.

The scattering pattern was observed on a viewing screen placed at a distance of $D = 40$ cm behind the crystal. In the steady state, an asymmetric diffusive scattering lobe extended from the transmitted pump beam in the direction opposite to the c-axis, as shown in figure 1. The detailed description of the spatial properties of the wide-angle PILS can be found elsewhere [1, 32].

The initial and the steady-state intensities of the scattering signal were measured for two exposure times $t = 0.1$ s and 300 s, respectively. A photodetector with an angular aperture of $\Delta\theta_s = 0.5°$ was adjusted in the plane of incidence at a fixed angle of $\theta_s = 15°$ (measured in air). Comparing the results of samples with different thicknesses it was found that the stationary PILS intensity $I_s(\theta_s)$ increased for samples with larger thickness L. At the same time the initial scattering intensity $I_{so}(\theta_s)$ decreased. The normalized coherent noise intensity as a function of L is shown in figure 3 in a logarithmic plot justifying equation (6). A fit yields an absorption coefficient of $\alpha = 2.1$ cm^{-1} which is well comparable to the value determined from the absorption spectrum.

The thickness dependence of the amplification coefficient m_s is shown in figure 4. The experimental results are given by markers. The dashed and solid lines correspond

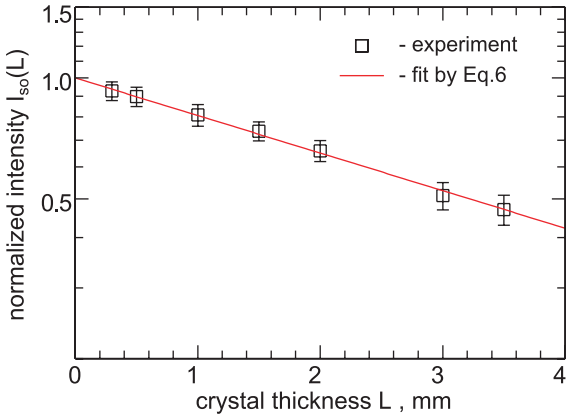

Figure 3. Thickness dependence of the initial scattering intensity in SBN:Ce. The fit with equation (6) corresponds to $\alpha = 2.1$ cm^{-1}.

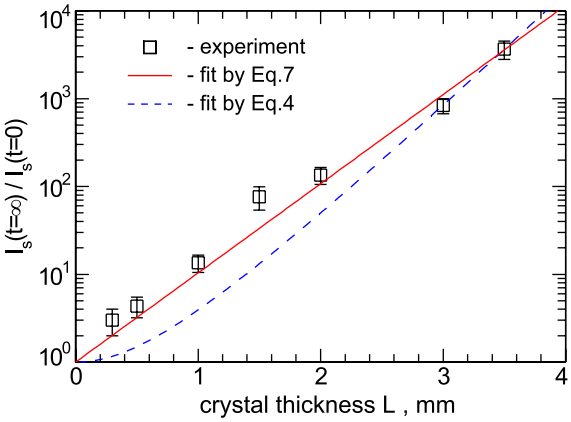

Figure 4. Thickness dependence of the scattering amplification coefficient m_s. The fitting with equation (4) and equation (7) gives $\Gamma = 23.3$ cm^{-1} and 32.2 cm^{-1}, respectively.

to fits of equation (4) and equation (7) to the data set, respectively. The best agreement is found for the curve of the *near-surface* scattering model. The fit yields a gain factor Γ of (23.3 ± 1.6) cm^{-1} (equation (7)) and of (32.2 ± 1.2) cm^{-1} (equation (4)). For comparison, two-beam coupling measurements were performed with a SBN sample with thickness $L = 1$ cm. An additional weak probe beam of intensity $I_{pr} = 0.005 \cdot I_p$ was adjusted at an angle of $\theta_s = 15°$ with respect to the pump beam. The gain factor was determined to be $\Gamma \approx 20$ cm^{-1}, which is in good agreement with the fitting results in figure 4 according to the *near-surface* scattering model. Our experimental data therefore indicate that PILS is composed from scattering components emerging from the crystal's near-surface or surface frontier to the pump beam. This accords well with previous suggestions presented in [1, 23]. It should be noted that a minor contribution of bulk scattering was concluded in [18], as well. This conclusion was obtained from numerical simulations of the scattering intensity profile, because a linear dependence on the crystal thickness was assumed for the bulk scattering; in contrast to an exponential one for the surface scattering.

Recently, it was shown that the scattering in SBN:Ce is strongly dependent on the polar structure of the crystal [24, 25].

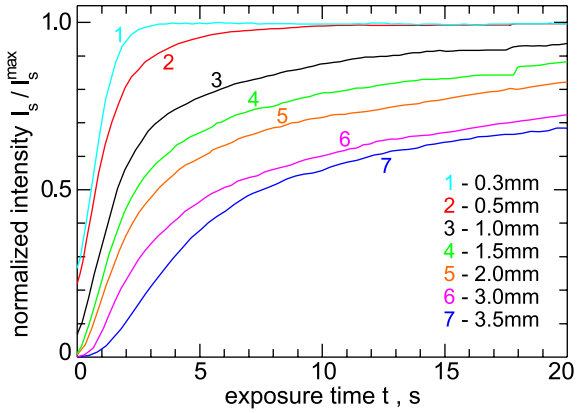

Figure 5. Dynamics of the wide-angle PILS in different SBN:Ce samples. A pronounced deceleration is revealed with increasing sample thickness.

In particular, the coherent noise (initial scattering) exhibits drastic changes in the vicinity of the phase transition and at the presence of an external electric field E_o having a magnitude of the electric coercive field. Obviously, coherent noise arising from the crystal surface does not possess any remarkable dependence on the polar structure. Therefore, the sources for coherent noise initiating PILS should be located within the crystal bulk and not on its surface. As a model attempt for SBN, the scattering sources were interpreted as local changes of the refractive index δn which are induced by internal (electric) fields and which are incorporated into the domain structure. Taking into account these results and the results of our present study we can conclude that the major contribution to PILS is from coherent noise scattered in the near-surface region of the crystal frontier to the pump beam.

Let us now discuss the competition between index gratings recorded by noisy waves related to the near-surface and the ones related to bulk scattering centers in more detail. The initial scattering intensity I_{so} of noisy waves from the near-surface region is assumed to be large compared with the ones originating in the bulk. At the same time the coupling strength Γl is larger for index gratings related to *near-surface* scattering centers since the interaction length can be approximated with the crystal thickness, i.e., $l \equiv L$. According to equation (1) these two factors ensure a significant enhancement of gratings recorded by the waves originating in the near-surface region. At the same time, grating recording with noisy waves appearing in the bulk is suppressed. As a result of this competition a deceleration of the scattering build-up dynamics can be assumed. According to these considerations, the deceleration should be more pronounced in thicker samples.

We therefore studied the scattering dynamics as a function of the crystal thickness in SBN:Ce. Figure 5 shows the scattering intensity normalized to the stationary value I_s^{max} as a function of the exposure time. The characteristic time τ_s of the scattering development was determined by fitting of the increasing part of the $I_s(t)$-curves to an exponential function: $I_s(t) \sim e^{t/\tau_s}$. A significant deceleration of τ_s by a factor of 25 with increasing thickness L is found. Figure 6 shows the resulting nonlinear thickness dependence of τ_s, which can be

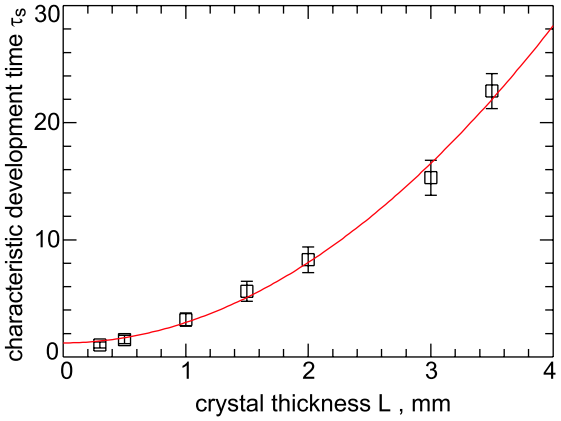

Figure 6. Thickness dependence of the characteristics time τ_s of the scattering dynamics. The best fit with a function $\tau_s = \tau_{di} + aL^b$ (equation (1)) is shown for $\tau_{di} = 1.2$ s, a =1.74 and $b = 1.98$.

fitted by the empirical function

$$\tau_s = \tau_{di} + aL^b, \tag{8}$$

where a, b and τ_{di} are fitting parameters. It is remarkable that the best fit corresponds to a nearly quadratic function in L, $\tau_s = \tau_{di} + 1.74 \cdot L^{1.98}$. Some retardation of the recording process can be expected due to the energy exchange between the strong pump wave and weak scattering waves. However, the two-wave mixing theory predicts a linear dependence of the characteristic recording time on the crystal thickness, $\tau_r \sim L$, taking into account the case of an interference pattern with varying contrast along the beam interaction [33]. We suggest that the explicitly pronounced nonlinear behavior of τ_s versus L revealed in our experiments can be assigned to the competition in the recording process of noisy photorefractive gratings. The Maxwell relaxation time $\tau_{di} = 1.2$ s is estimated from figure 6 by the extrapolation of the curve $\tau_s(L)$ to $L = 0$, when no grating competition takes place. The validity of this approach is justified by the independent experiment of the grating erasure performed for the same SBN sample in the two-beam setup. The directly measured value of τ_{di} is almost the same as that calculated with figure 6 and equation (8).

To verify the general character of the observed scattering behavior, equivalent experiments of the PILS phenomenon as a function of crystal thickness were performed for the *ee–ee* type scattering in $LiNbO_3$:Fe. The scattering was induced by two pump beams crossing the crystal as shown in figure 7(a). Previous experimental and theoretical studies revealed that a frequency shift $\Omega = \omega_{si} - \omega_p$ between the interacting waves enables efficient amplification of initially scattered waves [29]. The large photovoltaic effect, which is characteristic for $LiNbO_3$:Fe, typically causes a local photorefractive response. In this case, a small frequency shift $\Omega \approx 1/\tau_{di}(\sim 1\text{Hz})$ between the recording waves is required to achieve small-signal amplification with a non-zero gain factor Γ in the steady state. Such frequency detunings in the scattered light may originate, for instance, from temporal fluctuations of material parameters of the crystal. Therefore, scattering sources in $LiNbO_3$ are also associated with bulk rather than with surface inhomogeneities of the crystal.

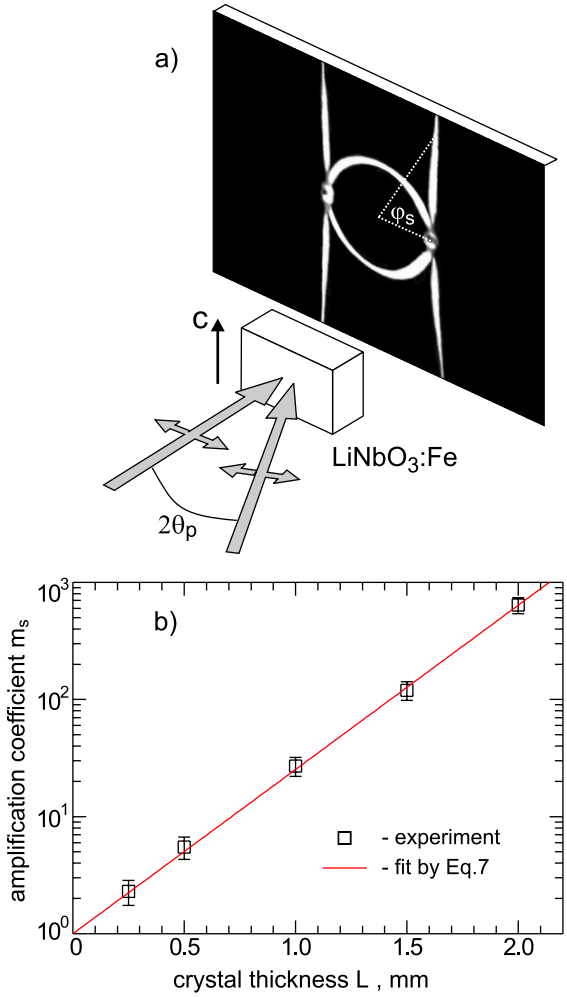

Figure 7. Observation of the parametric PILS of *ee–ee* type in $LiNbO_3$:Fe. (a) Experimental setup: two coherent beams ($\lambda = 514.5$ nm) of extraordinary polarization cross at the angle $2\theta_p = 15°$ orthogonally to the c axis. The scattering is monitored at the azimuth angle $\varphi = 60°$. (b) Thickness dependence of the scattering amplification coefficient m_s. $LiNbO_3$:Fe samples are of thickness 0.25, 0.5, 1, 1.5 and 2 mm. Theoretical fitting with equation (7) gives $\Gamma = 33.5$ cm^{-1}.

$LiNbO_3$ grown by the Czochralski technique from the congruently melting composition with 0.006 wt% of iron was used in our experiments. Five samples of different thicknesses from 0.25 to 2 mm were cut orthogonally to the a-axis. In the setup, the c-axis of the crystal is orthogonal to the plane of incidence. The angle between the two beams is given by $2\theta_p = 15°$ (measured in air). The intensity of each beam reaches nearly $I_p = 4$ W m^{-2}. The scattering pattern is observed on the viewing screen as a scattering ring and two vertical scattering arcs touching the pump beams. The incident and scattering light has the same extraordinary polarization in the crystal. The scattering intensity was monitored in the right arc at the azimuth angle $\varphi_s = 60°$ (see figure 7). The scattering dynamics in the ring revealed an increase of the deceleration with increasing sample thickness similar to that shown in figure 5. The scattering amplification coefficient m_s versus L measured for the scattering arc is plotted in

figure 7(b). Obviously, it resembles the results of figure 6. The fit yields a gain factor for the parametric *ee–ee* scattering of $\Gamma = (33.5 \pm 1.0)\ \mathrm{cm}^{-1}$, which is larger than for the wide-angle scattering in SBN:Ce. It confirms the conclusion of the model for the *ee–ee* scattering, which considers a large stationary gain factor Γ for frequency detuned scattered waves.

Thus, it becomes apparent that general features of the thickness dependence remain qualitatively the same regardless of the particular type of the photorefractive crystal and of the scattering process. This allows us to conclude that the dominating role in the formation of the stationary PILS pattern belongs to the scattering emerging from near-surface regions of the crystal. The amplification of bulk seed scattering is suppressed by near-surface scattering. It results in a slowing down of the PILS dynamics, which increases for thicker crystals. Therefore, the effective interaction length l in equation (1) can be approximated with the crystal thickness L with rather high fidelity. This is particularly valid for crystals with a large thickness $L \gg 1/\Gamma$.

4. Conclusion

The thickness dependence of wide-angle and parametric PILS is studied in the photorefractive crystals SBN:Ce and $LiNbO_3$:Fe, respectively. Two models of (i) *bulk* and *near-surface* scattering centers are comparatively discussed as the origin of the PILS phenomenon. Thereby, our study focuses on the interpretation of the interaction length in the nonlinear wave mixing process between noisy waves and an incident pump beam. We can conclude from the direct comparison of the theoretical model approach with the experimental study that the major contribution to PILS is given by the scattering originating in a thin region of the crystal frontier to the incident beam. It is shown that the crystal thickness L can be considered as the interaction length between the pump beam and scattered waves. A deceleration of the scattering dynamics with increasing thickness of the crystal is revealed. This finding is interpreted by the competition between differently recorded noisy photorefractive gratings, which is particularly important for scattering processes. It is shown that the reported features of PILS are quite general for different photorefractive crystals. Moreover, they do not depend on the particular type of scattering process. Our results are important from the viewpoint of possible applications of the scattering for contact-free material characterization [25, 32]. The obtained results may also be important for the analysis of coherent oscillation dynamics in different optical resonators with photorefractive crystals as a nonlinear medium.

Acknowledgments

The work is supported by the DFG (projects GRK 695 and IM37/2-1).

References

[1] Voronov V, Dorosh I, Kuz'minov Yu and Tkachenko N 1980 Photoinduced light scattering in cerium-doped barium strontium niobate crystals *Sov. J. Quantum Electron.* **10** 1346–9

[2] Smirnova T M and Tikhonov E A 1979 Conical scattering of laser beams in active dye solutions *Sov. J. Quantum Electron.* **9** 93–7

[3] Rupp R A and Dress F W 1986 Light-induced scattering in photorefractive crystals *Appl. Phys.* B **39** 223–9

[4] Kirilenko E K 1989 Some characteristics of formation of volume dynamic holograms by concurrent waves propagating in resonant atomic media *Sov. J. Quantum Electron.* **19** 930–3

[5] Imlau M, Woike Th, Schieder R and Rupp R A 1999 Holographic scattering in centrosymmetric $Na_2[Fe(CN)_5NO]\cdot 2H_2O$ *Phys. Rev. Lett.* **82** 2860–3

[6] Khoo I C and Liang Y 2000 Stimulated orientational and thermal scatterings and self-starting optical phase conjugation with nematic liquid crystals *Phys. Rev.* E **62** 6722–33

[7] Feinberg J 1982 Asymmetric self-defocussing of an optical beam from the photorefractive effect *J. Opt. Soc. Am.* **72** 46–51

[8] Obukhovski V and Stoyanov A 1985 Photoinduced light scattering in crystals with a nonlocal response *Sov. J. Quantum Electron.* **15** 367–71

[9] Kiseleva I N, Obukhovskii V V and Odoulov S G 1986 Parametric scattering of the holographic type in class 3 m crystals *Sov. Phys.—Solid State* **28** 1673–6

[10] Sturman B I, Odoulov S G and Goulkov M Yu 1996 Parametric four-wave processes in photorefractive crystals *Phys. Rep.* **275** 197–254

[11] Joseph J, Pilai P K C and Singh K 1990 A novel way of noise reduction in image amplification by two-beam coupling in photorefractive $BaTiO_3$ crystal *Opt. Commun.* **80** 84–8

[12] Breugnot S, Dolfi D, Rajbenbach H and Huignard J-P 1994 Enhancement of the signal-to-background ratio in photo-refractive two-wave mixing by mutually incoherent two-beam coupling *Opt. Lett.* **19** 1070–2

[13] Neumann J, Mendricks S, Krätzig E, Goul'kov M and Odoulov S 1998 Photorefractive light amplification by forward four-wave mixing in $BaTiO_3$ *Opt. Commun.* **146** 220–4

[14] Odoulov S 1989 Vectorial interaction in photovoltaic media *Ferroelectrics* **92** 213–25

[15] Goulkov M, Granzow T, Dörfler U, Woike Th, Imlau M and Pankrath R 2003 Temperature dependent determination of the linear electrooptic coefficient r_{33} in $Sr_{0.61}Ba_{0.39}Nb_2O_6$ single crystals by means of light-induced scattering *Opt. Commun.* **218** 173–82

[16] Goulkov M, Imlau M, Pankrath R, Granzow T, Dörfler U and Woike Th 2003 Temperature study of photoinduced wide-angle scattering in cerium-doped strontium barium niobate *J. Opt. Soc. Am.* B **20** 307–13

[17] Imlau M 2007 Photorefraction and defects: a relation with mutual benefit *Phys. Status Solidi* a **204** 642

[18] Segev M, Engin D, Yariv A and Valley G C 1993 Temporal evolution of fanning in photorefractive materias *Opt. Lett.* **18** 956–8

[19] Xie P, Hong Y-H, Dai J-H, Zhu Y and Zhang H-J 1993 Theoretical and experimental studies of fanning effects in photorefractive crystals *J. Appl. Phys.* **74** 813–8

[20] Zozulya A A, Saffmann M and Anderson D Z 1994 Propagation of light-beams in photorefractive media—fanning, self-bending, and formation of self-pumped 4-wave-mixing phase-conjugation geometries *Phys. Rev. Lett.* **73** 818–21

[21] Snowbell M, Horowitz M and Fischer B 1994 Dynamics of multiple two-wave mixing and fanning in photorefractive materials *J. Opt. Soc. Am.* B **11** 1972–82

[22] Parshall E, Cronin-Golomb M and Barakat R 1995 Model of amplified scattering in photorefractive media: comparison of numerical results and experiment *Opt. Lett.* **20** 432–4

[23] Kamshilin A A, Raita E and Khomenko A V 1996 Intensity redistribution in a thin photorefractive crystal caused by strong fanning effect and internal reflections *J. Opt. Soc. Am.* B **13** 2536–43

[24] Goulkov M, Granzow T, Dörfler U, Woike Th, Imlau M and Pankrath R 2003 Study of beam-fanning hysteresis in photo-refractive SBN:Ce: light-induced and primary scattering as functions of polar structure *Appl. Phys.* B **76** 407–16

[25] Goulkov M, Shinkarenko O, Granzow T, Woike Th and Imlau M 2004 Beam fanning used to study thermal disorder and decay of polar structures in the ferroelectric relaxor $Sr_{0.61}Ba_{0.39}Nb_2O_6$ *Europhys. Lett.* **66** 48–54

[26] Kukhtarev N, Markov V, Odoulov S, Soskin M and Vinetskii V 1979 Holographic storage in electrooptic crystals. II. Beam coupling—light amplification *Ferroelectrics* **22** 961–4

[27] Imlau M, Bastwöste K, Möller S, Voelker U and Goulkov M 2006 Dispersion of the electro-optic properties of cerium-doped $Sr_{0.61}Ba_{0.39}Nb_2O_6$ *J. Appl. Phys* **100** 053110

[28] Goulkov M, Odoulov S, Woike Th, Imbrock J, Imlau M, Krätzig E, Bäumer C and Hesse H 2002 Holographic light scattering in photorefractive crystals with local response *Phys. Rev.* B **65** 195111

[29] Sturman B, Goulkov M and Odoulov S 1993 Polarization-degenerate parametric light scattering in photorefractive crystals *Appl. Phys.* B **56** 193–9

[30] Sturman B I and Fridkin V M 1992 *The Photovoltaic and Photorefractive Effects in Nonsymmetric Materials* (New York: Gordon and Breach)

[31] Granzow T, Dörfler U, Woike Th, Wöhlecke M, Pankrath R, Imlau M and Kleemann W 2001 Influence of pinning effects on the ferroelectric hysteresis in cerium-doped $Sr_{0.61}Ba_{0.39}Nb_2O_6$ *Phys. Rev.* B **63** 174101

[32] Imlau M, Goulkov M, Fally M and Woike Th 2005 Characterization of polar oxides by photo-in-duced light scattering *Polar Oxides: Properties, Characterization and Imaging* (Weinheim: Wiley–VCH)

[33] Sturman B I 1978 Interaction of two light waves in a crystal caused by photoelectron diffusion and drift *Sov. Phys.—Tech. Phys.* **23** 589–95